Comprehensive Analysis of the Hydrogen Bond Network Morphology and OH Stretching Vibrations in Protonated Methanol−Water Mixed Clusters, $H^+(MeOH)_1(H_2O)_n$ ($n = 1-8$)

Jer-Lai Kuo,*,† Zhi-zhong Xie,† Dan Bing,† Asuka Fujii,*,‡ Toru Hamashima,‡ Ken-ichiro Suhara,‡ and Naohiko Mikami‡

School of Physical and Mathematical Sciences, Nanyang Technological University, Singapore 637371, Singapore, and Department of Chemistry, Graduate School of Science, Tohoku University, Sendai 980-8578, Japan

Received: June 30, 2008; Revised Manuscript Received: August 9, 2008

Density functional theory (DFT) calculations of protonated methanol−water mixed clusters, $H^+(MeOH)_1(H_2O)_n$ ($n = 1-8$), were extensively carried out to analyze the hydrogen bond structures of the clusters. Various structural isomers were energy optimized, and their relative energies with zero point energy corrections and temperature dependence of the free energies were examined. Coexistence of different morphological isomers was suggested. Infrared spectra were simulated on the basis of the optimized structures. The infrared spectra were also experimentally measured for $n = 3-9$ in the OH stretching vibrational region. The observed broad bands in the hydrogen-bonded OH stretch region were assigned in comparison with the simulations. From the DFT calculations, the preferential proton location was also investigated. Clear correlations between the excess proton location and the cluster morphology were found.

I. Introduction

Recent development of spectroscopic measurements and theoretical calculations has successfully unveiled structures of various hydrogen-bonded clusters, which are important models for solvations in the condensed phases.[1−3] Protonated water and methanol clusters, $H^+(H_2O)_n$ and $H^+(MeOH)_m$, have especially been studied in detail up to the large sizes ($n = 100$ and $m = 17$, respectively) because of their fundamental importance in understanding of the hydrogen bond network structure as well as the proton solvation in the protic solvent.[4−26] The tetrahedral 4-coordination nature of water leads to the morphological development of protonated water clusters from the 1-D chains to the 3-D polyhedral cages via the 2-D net structures. This evolution has been confirmed by infrared (IR) spectroscopy, and the size and temperature dependence of the preferential network morphology has been discussed on the basis of the extensive theoretical calculations.[4−22] On the other hand, the maximum coordination number of methanol is limited to 3, and it restricts the morphology of protonated methanol clusters to much simpler one.[23−26] Topological consideration on the morphology of the protonated methanol clusters demonstrated that the "bicyclic" structures are the terminal of their morphological development, and the IR spectroscopic studies and theoretical calculations have also supported the preference of the simple network morphology in the protonated methanol clusters.[25,26]

In spite of the very different preferences of the hydrogen bond network morphology, bulk water and methanol seem to mix each other at an arbitrary ratio. However, mass spectrometry of liquid beams, neutron diffraction, and X-ray emission studies strongly suggested that the water and methanol moieties in the mixed solution are separated from each other in the microscopic level.[27−29] Gas-phase mixed clusters would give us a much clearer picture on the microscopic mixing between the two components. Along with this line, there have been many mass spectrometric studies on the protonated methanol−water mixed clusters, $H^+(MeOH)_m(H_2O)_n$, abbreviated to $H^+M_mW_n$ in the following.[30−38] It is, however, difficult to extract direct information on the hydrogen bond structure from the mass spectrometric measurements, except some proposals of the specific magic number structures. For example, the mass spectrometric study by Castleman, Jr., and co-workers suggested that $H^+M_mW_n$ ($m < 10$, $m + n = 21$) forms the similar cage as H^+W_{21}.[34,35] Chang and co-workers carried out the pioneering IR spectroscopic study on $H^+M_mW_n$ at the small sizes [($m = 1$, $n = 1-6$), ($m = 4$, $n = 1$), and ($m + n = 4$)] and succeeded to determine the preferential hydrogen bond network structures in combination with the density functional theory (DFT) calculations.[39−42] As for the much larger sized clusters, we observed the IR spectra of $H^+M_mW_n$ in the wide size range ($m = 1-4$, $n = 4-22$) and proved the completion of the 3-D polyhedral cage formation at $m + n = 21$ in the mixed clusters[43] that was first proposed by the mass spectrometric study.[34,35] In these IR spectroscopic studies, small but definite frequency shifts of the dangling OH stretching vibration bands played a key role to extract the hydrogen bond structure information. On the other hand, the hydrogen-bonded OH stretching bands were so broadened that their assignments have not yet been fully examined, though size dependent spectral shifts are seen in the clusters of $m + n \lesssim 10$.

The preferential location of the excess proton is another highly important issue in protonated mixed clusters.[39−45] The magnitudes of the gas-phase proton affinities (PA) of isolated molecules are not necessarily reliable indexes to predict the preferential location of the excess proton between two components because of the stabilization with the solvation. For example, dilute aqueous methanol is weakly acidic though the PA of methanol (180 kcal/mol) is higher than that of water (165 kcal/mol). [46] To experimentally probe the excess proton location, fragmentation mass spectrometry had been regarded as the unique method. For $H^+M_mW_n$ ($m \gg n$), the major fragment channel changes from water loss to methanol loss with increase

* To whom correspondence should be addressed. E-mail: jlkuo@ntu.edu.sg (J.-L.K.); asukafujii@mail.tains.tohoku.ac.jp (A.F.).
† Nanyang Technological University.
‡ Tohoku University.

10.1021/jp8057299 CCC: $40.75
Published on Web 09/25/2008

of the cluster size, and it was proposed that the ion core switching from the $MeOH_2^+$ core to the H_3O^+ core occurs to form a specific inclusion structure.[30−38] Later on, IR spectroscopic studies on the proton location in various protonated mixed clusters were extensively carried out by Chang and co-workers, and they observed the coexistence of the $MeOH_2^+$ and H_3O^+ ion cores in $H^+M_mW_n$ [($m = 4$, $n = 1$), ($m+n = 4$), and ($m = 1$, $n = 3-5$)].[39−42] On the other hand, in the theoretical analysis of the compatibility of methanol and water in the hydrogen bond network of the large cluster ($n + m = 21$), we found that the $MeOH_2^+$ core is no longer stable and that H_3O^+ moiety dictates the dodecahedral cage cluster structures.[43] This gives rise to a question when the coexistence of the two types of the ion core changes to the clear preference of the H_3O^+ ion core. In the previous study, we also examined the proton location in $H^+M_1W_7$ and found that the protonated methanol core is stable only in the noncubic structures.[43] These results suggest the correlation between the cluster morphology and the preferential location of the excess proton, though the systematic study has not yet been performed.

In the present work, we carry out DFT calculations on stable structures of various morphologies and corresponding IR spectra of $H^+M_1W_n$ ($n = 1-8$). Part of them ($n = 1-6$) have been studied by Chang and co-workers,[40] but we employed more extensive and systematic approaches to survey possible structures. Relative energies of isomers and temperature dependence of the preferential structures are examined by the calculations. IR spectra in the hydrogen-bonded and dangling OH stretch region are simulated on the basis of the optimized structures. The size-selected IR spectra of the $n = 7-9$ clusters are also experimentally observed by infrared dissociation spectroscopy. In addition, those of $n = 3-6$, which have first been reported by Chang and co-workers,[40] are remeasured for convenience of the comparison with the theoretical simulations. The hydrogen-bonded OH stretch features in the observed IR spectra, which show moderate size dependence, are analyzed in comparison with the simulations. The preferential location of the excess proton is also systematically examined from the chain like type clusters to the three-dimensional cage type clusters. The correlation between the excess proton location and cluster morphology is discussed.

II. Computational Methods

1. Quantum Chemical Methods. All the DFT calculations reported in this work were carried out using the commercial Gaussian 03 program package.[47] We optimized the geometries without any symmetry constraints at the B3LYP level of computations with the 6-31+G* basis set. The reliability of this level of calculations for protonated clusters has been well established by previous studies.[5,9−11,39−43] For each energy-optimized structure, the frequency calculation was performed to confirm the geometry is an energy minimum, and the zero point energy (ZPE) correction is estimated by the harmonic approximation ($ZPE \cong \Sigma_i \hbar_i \omega/2$). To access thermal effects, we also calculated the Gibbs free energy at various temperatures up to 200 K.

2. Structure Survey of $H^+M_1W_n$. To construct a wide variety of input structures of $H^+M_1W_n$ for the DFT study, we have engaged the following two approaches. For small sizes, only linear, tree, and cyclic structures can be formed, and these structures can be constructed manually. Wu et al. have taken this approach and carried out a rather comprehensive search for up to $n = 4$.[40] Following their examples, we have also built all the possible linear, tree, and cyclic structures for $n \leq 4$ with the hope to observe some systematic trends and then use these empirical rules to build larger clusters.

Such an ad hoc method is limited only to smaller clusters, because both the complexity in the morphology and the number of chemically acceptable conformations within a given morphology increase exponentially with respect to the cluster size. For medium-sized clusters (that $n \approx 5$ or 6), an exhaustive search is no longer practical, we have, therefore, relied on our previous experience with protonated water clusters H^+W_n to construct $H^+M_1W_n$ isomers; that is, a $H^+M_1W_n$ can be easily obtained by replacing an acceptor−donor (AD) or double acceptor-single donor (AAD) water by a methanol from their structural cousin of H^+W_{n+1}.[43]

III. Experimental Methods

IR spectra of the $H^+M_1W_n$ cluster cations were recorded by IR predissociation spectroscopy using a mass spectrometer that was equipped with linearly aligned tandem quadrupole mass filters connected by an octopole ion guide. The details of the apparatus have already been described in the previous papers,[7,25,43] and only a brief description is given here. $H^+M_1W_n$ was produced by a photoassisted discharge of the methanol/water mixed vapor seeded in the Ne buffer gas (total pressure of 3 atm). The gaseous mixture was expanded from a pulsed supersonic valve through a channel nozzle. The channel was equipped with a pin electrode at its sidewall, and a direct current voltage of −300 V relative to the channel was applied to the electrode. The discharge in the channel was triggered by irradiation of the electrode surface with a laser pulse (355 nm, 5 mJ/pulse), which is synchronized with the pulsed valve operation. The $H^+M_1W_n$ cluster cations were cooled through the expansion from the channel. The cluster cations were size-selected by the first quadrupole mass filter, and then they were introduced into the octopole ion guide. The mass resolution of the first mass filter was set to be high enough to exclude the contamination of undesired cluster species. Within the octopole ion guide, the size-selected clusters were irradiated by a counter propagating IR laser and were sent to the second quadrupole mass filter, which was tuned to pass only the mass of the $H^+M_1W_{n-1}$ fragment ion produced by the vibrational excitation. Thus, an IR spectrum of the size-selected cluster was recorded by monitoring the fragment ion intensity while scanning the IR laser frequency. The IR light was generated by an infrared optical parametric oscillator (Laser Vision) pumped by the fundamental output of a YAG laser (Continuum Powerlite 8000).

IV. Results and Discussion

1. Morphologies of the Mixed Clusters.

A. Construction of Structures of Small Isomers of $H^+M_1W_n$ $n \leq 4$ or 5. For $H^+M_1W_{n \leq 4}$, only linear (L_n), tree (T_n), and cyclic (C_n and Ct_n) structures can be formed (n represents the number of the water molecules in the cluster), and we have carried out an exhaustive search on all the possible conformations within each morphology. The most stable conformation in each morphological type is shown in Figure 1 along with their relative energies E_0. The values in the parentheses are the ZPE corrected energies (E_o +ZPE). The zero of these energy scales are set to the energies of the most stable isomers in each cluster size.

Linear Structures (L_n). Linear (L_n) structures are the most basic form and they exist for $n \geq 2$. Only the most stable L_n structure in each cluster size is shown in Figure 1, and all the L_n structure that are stable after the geometry optimization are tabulated in Supporting Information. It is obvious that the stable conformation tends to have the $MeOH_2^+$ ion core in the center

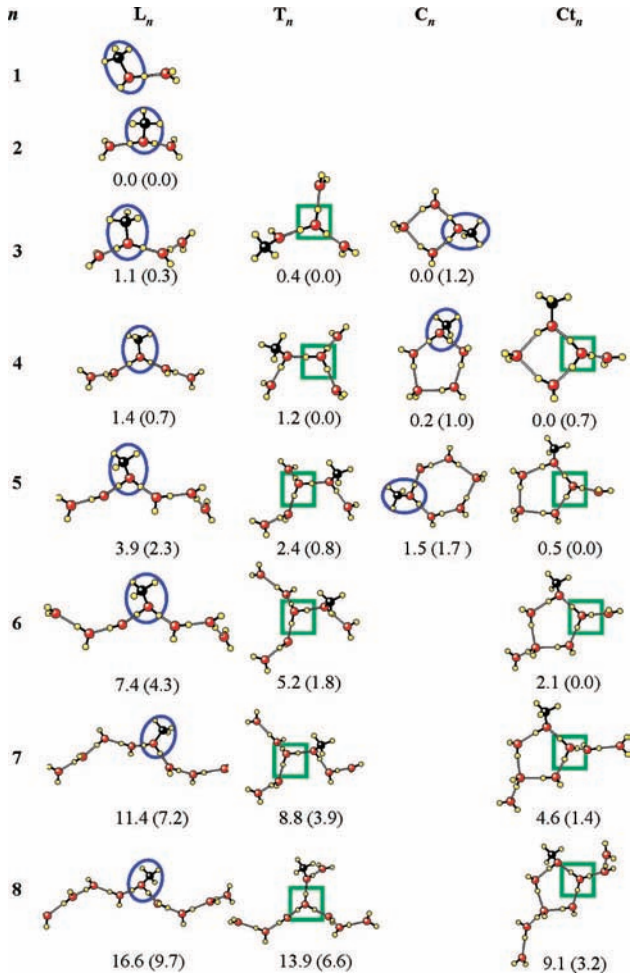

Figure 1. The most stable structures of the linear (L_n), tree (T_n), and cyclic (C_n and Ct_n) forms of $H^+(MeOH)_1(H_2O)_n$ ($H^+M_1W_n$) and their relative energies (E_0) in kcal/mol. The values in the parentheses are the ZPE-corrected relative energies (E_0 + ZPE). The zero of these energy scales is set to the energy of the most stable isomer of each size. The positions of the methanol/water ion core are highlighted with the blue circles/green squares, respectively. The complete list of the isomers is seen in Supporting Information.

of the cluster. It is interesting to note that the similar trend was seen in H^+M_m in our previous study.[26] While conformations with the H_3O^+ ion core also can be stable as local minima, they are about 3 kcal/mol higher in E_0 than the most stable linear form. Since this trend is confirmed for up to $n = 5$, we have used this empirical rule to construct representatives for the L_n clusters of $n \geq 5$.

Tree Structures (T_n). Tree structures are more complicated than the linear forms. We have examined a very extensive array of conformations within the T_n family and only selected isomers are depicted in Figure 1. A complete list of the tree structures can be found in Supporting Information. Within the T_n family, isomers can have branches of different length; we use a three-digit label to indicate the length of their three branches. In the present study, we found that isomers with more evenly distributed branches tend to be more stable. For example in $H^+M_1W_7$, the 222 isomers are more stable than the 321 isomers. This trend is further confirmed in $H^+M_1W_8$ in which we can see that 322 isomers are more stable than the 331, 421, and 511 isomers.

While both kinds of the ion cores are geometrically possible in tree structures, isomers with H_3O^+ in the center seem to be energetically favored because the triple proton-donation nature of H_3O^+ is advantageous to form the branching site of the T_n structures. The $MeOH_2^+$ ion core can be stable only in isomers with one exceptionally long branch. Therefore, it would be reasonable to suppose that the H_3O^+ ion core is preferred in larger tree structures. Furthermore, there is a clear tendency for the MeOH moiety to stay close to the ion core. This trend is easy to understand as the proton affinity of MeOH is larger than that of H_2O.[46]

Cyclic Structures (C_n and Ct_n). Simple cyclic structures can be divided into two categories. In the first kind, two terminal molecules of a L_n structure are bound to each other. The binding site becomes a double acceptor (AA) site (we call this type structure C_n). In the second category, the hydrogen bond network in the ring is further extended by branching out a "tail" (we call them Ct_n).

We have built all possible conformations of C_n structures starting with the 3-member ring. Only one 4-member and two 5-member rings survive after the geometrical optimization. Our search result agrees with the findings by Wu et al., though they listed only the most stable forms.[40] We have further constructed 6-member ring structures and have located three stable structures. We found two empirical rules for the C_n structures: (1) the $MeOH_2^+$ ion core seems to be preferred, and (2) the AA water prefers to be away from the ion core.

Structural isomers of Ct_n were built by adding one or more water molecules to the different positions on the above-mentioned C_n structures. We found the following trends: (1) the ion core seems to have different preference depending on the ring-size; that is, H_3O^+ is preferred in 5- and 6-member rings and $MeOH_2^+$ in the 4-member ring. This is consistent with the fact that the H−O−H angle in $MeOH_2^+$ is smaller than the H−O−H angle in H_3O^+; therefore in small-sized rings, $MeOH_2^+$ would result in less stress and more stable structures. (2) Similar to the T_n structures, the MeOH site also tends to stay close to the ion core.

B. Isomers of More Complicated Morphologies Deriving from $H^+(H_2O)_{n+1}$. Isomers of more complicated morphologies are derived from protonated water clusters. It has been shown that hexamer and larger protonated water clusters exhibit multicyclic forms, and cubic and other cagelike structures are stable for octamers or larger clusters as low-energy minima.[16] Our strategy here is to select the most stable conformation within each of above-mentioned morphology on the basis of our previous studies on the protonated water clusters and use them for a systematic study on the effect of replacement to a methanol molecule at different locations.[16]

Bicyclic Structures (bC_n for $n \geq 5$) and Tricyclic Structures (tC_n for $n \geq 6$). When two sites in a cyclic structure are bridged by a hydrogen bond chain, the structure develops into a bicyclic (bC_n) structure. More hydrogen bonds segment the hydrogen-bonded ring with increase of the size, and then the morphology is categorized into the tricyclic structure (tC_n). Because of the strategy we adapted, our initial input structures contain only the H_3O^+ ion core, and proton transfer occurs frequently during the geometry optimization. For isomers, in which the MeOH and H_3O^+ sites are far away from each other, we have also attempted to pull the proton along different possible transfer pathways and have found that the proton can also relax to the more stable position with our method. The most stable structures of the bC_n family are shown in Figure 2, and we found the following trends: (1) MeOH has a tendency to stay as close to the ion core as possible. Between 2- and 3-coordinated sites, the former is preferred. (2) Both forms of the ion core seem to coexist, and there is no clear preference. The $MeOH_2^+$ ion core

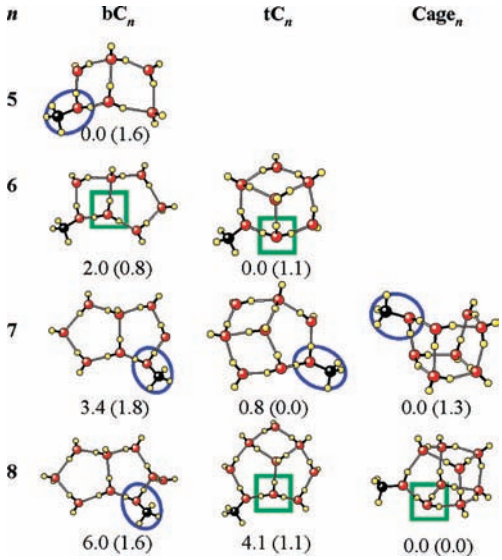

Figure 2. The most stable structures of the bicyclic (bC$_n$), tricyclic (tC$_n$), and cage structures (Cage$_n$) of $H^+M_1W_n$ and their relative energies (E_0) in kcal/mol. The values in the parentheses are the ZPE-corrected relative energies (E_0 + ZPE). The zero of these energy scales is set to the energy of the most stable isomer of each size. The positions of the methanol/water ion core are highlighted with the blue circles/green squares, respectively. The complete list of the isomers is seen in the Supporting Information.

is found to be stable only on 2-coordinated sites. Though we have attempted to construct a few isomers with $MeOH_2^+$ sitting on a 3-coordinated site, none of them survives upon the geometry optimization.

When the hydrogen bond network in bC$_n$ or tC$_n$ is further extended by branching out a "tail", the morphology would be categorized into bCt$_n$ or tCt$_n$, respectively. We found, however, the energies of bCt$_n$ and tCt$_n$ are higher than those of bC$_n$ and tC$_n$ at the same size (see Supporting Information).

Cage Structures (Cage$_n$ for $n \geq 7$). In the octamer ($1 + n = 8$) or larger, 3-D cage structures can be formed. The choice of the ion core becomes very simple in the cage structures. Only the H_3O^+ ion core is found to be stable. This finding is inline with the observation we noticed for bC$_n$ and tC$_n$ that $MeOH_2^+$ can be stable on 2-coordinated sites, which are missing in polyhedral cages. As is the other structures, the MeOH site tends to stay close to the ion core and prefers the 2-coordinated sites.

2. Relative Stabilities of the Isomer Structures. We have performed the geometry optimizations on a wide variety of structural isomers. Their relative stabilities of all the isomers we have examined are summarized in Figure 3. The distribution of the electronic energies (E_0), ZPE, and total energies (E_0 + ZPE) of isomers is shown for each cluster size ($n = 5-8$). The isomers are categorized by their morphologies and are arranged from left to right roughly following the "compactness" of the morphology. In each cluster size, the energy of the most stable isomer (or the smallest correction term) is set to zero of the energy scale of each item. Some general trends are clearly seen from the figure, as summarized below.

The electronic energy E_0 is depicted in the left-most column, and it shows a systematical trend favoring the more compact structures. This trend becomes very clear for $n = 7$ and 8, and it is inline with the simple bond counting concept as there are more hydrogen bonds in the more compact structures. On the other hand, it is obvious from the middle column that the ZPE terms show the opposite trend favoring the open structures. This is attributed to the trend that more compact structures have

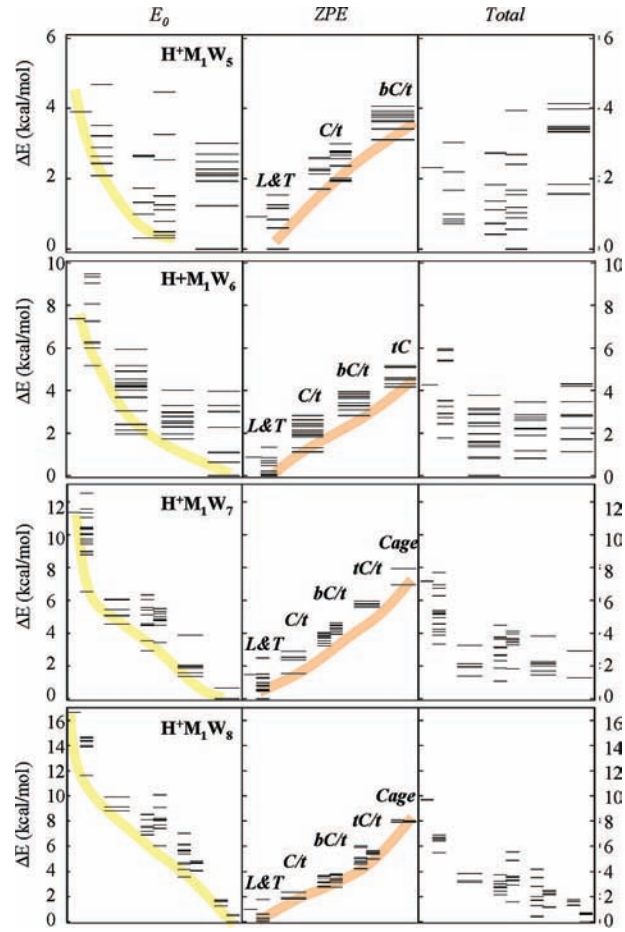

Figure 3. Relative energetics of all the structural isomers of $H^+M_1W_n$ computed at B3LYP/6-31+G*. Electronic energy (E_0), ZPE correction term (ZPE), and the total energy at the zero vibrational level (E_0 + *ZPE*) are summarized in the figure. Morphologies with and without a "tail" are grouped together. For example, C/t includes both of C$_n$ and Ct$_n$. The energies of isomers in the same morphology are compiled in a column, and the morphologies are arranged roughly following their "compactness", that is, from the most "open" structure on the left to the most "compact" one on the right. The stripes are made for eye-guiding purposes to illustrate the trends in E_0 and ZPE.

higher vibrational frequencies, reflecting their more rigid structures. For $n = 5-8$, the difference in ZPE among the different morphologies can be as large as 4 kcal/mol, and it is comparable or sometimes larger than the difference in E_0. Because of the compensation between E_0 and ZPE, the total energy (E_0 + ZPE), which means the relative stability at 0 K, shows no clear dependence on the morphology. In fact, these energies are very close to each other (less than 1 kcal/mol) for $n = 5-8$. Within the accuracy of the present calculations, it is not reliable to make an unambiguous assignment on the global minimum isomer.

It is interesting to see that the difference of ZPE among isomers (ΔZPE) exhibits a more quantitative trend than those in E_0. For example, ΔZPE between L$_n$/T$_n$ and C$_n$/Ct$_n$ is about 1 kcal/mol. ΔZPEs are found to be about 3 and 4 kcal/mol for L$_n$/T$_n$ − bC$_n$ and L$_n$/T$_n$ − tC$_n$, respectively. This survey helps to quantify the influence of ZPE to determine the relative stabilities among the different morphologies. Moreover, these values would be able to use for future studies on much larger protonated clusters, of which evaluation of the second derivatives (vibrational frequencies) becomes too costly.

3. Thermal Effects Accessed via the Gibbs Free Energy. It has been shown that the entropic effect is rather significant in determining the most probable structure of hydrogen-bonded clusters at realistic experimental temperatures.[9,16,22,26,48−51] For example, Monte Carlo simulations on neat protonated water clusters indicate large-amplitude motion is prevalent at temperature above ∼100 K.[16,49−51] However, nuclear quantum effects were not included in such classical simulations, and the ZPE correction alters the relative stability. In this work, we use the Gibbs free energy based on the harmonic approximation at various temperatures as an economical alternative way to include both the entropic and nuclear quantum effects. We should note here that the thermal simulations have proven that the structures of small/medium-sized hydrogen-bonded clusters may undergo significant structural changes with elevation of the temperature.[16,49−51] Therefore, the estimated Gibbs free energy shown here should be only taken as guidance for the qualitative trend, and it should not be used as a definite criterion for selecting the most probable structure at an elevated temperature.

Another issue is the existence of too many orientational isomers within a given morphology. This would complicate our analysis here. Therefore we have selected the most stable conformation as the representative. We use the Gibbs free energy of the most stable cyclic structure as the reference and the temperature dependence of the Gibbs free energies of the representatives are summarized in Figure 4. It is clear that the entropy favors the open structures. For example, the relative Gibbs free energies of L_n and T_n structures decrease as the temperature rises. The Gibbs free energies of the compact structures show the opposite trend, and the steepness of the free energy is consistent with the compactness of the structures. Furthermore, the profound entropic effect is demonstrated in $H^+M_1W_8$ by the following example. At zero K, the tree structure is less stable more than 6 kcal/mol in comparison with the cage structure, but at 200 K, both of them have nearly the same free energy.

4. Simulations of IR Spectra in 3000−3800 cm^{-1}. The IR spectra of $H^+M_1W_n$ in the 3-μm region can be divided into two ranges. Above 3600 cm^{-1}, bands come from the free (dangling) OH stretching vibrations, and those in between 3000 and 3600 cm^{-1} are due to hydrogen-bonded OH stretches. The former has been extensively examined by Chang and co-workers.[40,42] It has been shown that the free OH frequency is very sensitive to the coordination of the site. In the small-sized protonated water and mixed clusters, the free OH stretch region has been studied as a key for the isomer structure determination, and the morphological development of the large-sized protonated water clusters has also been elucidated by the size-dependent behavior of the free OH stretch region.[5−11] On the other hand, the hydrogen-bonded OH region has not yet been fully examined, though the moderate size-dependence is seen in the IR spectra. Therefore, we focus mainly on the spectral behavior of the hydrogen-bonded OH stretches in this study. Chang and co-workers have shown that the free OH stretch bands of protonated clusters are successfully reproduced by B3LYP/6-31+G* level calculations with the scaling factor of 0.973.[5,9−11,39−42,52−54] We also employ the same calculation level and scaling factor to analyze hydrogen-bonded OH stretch modes. The simulated IR spectra of the most stable isomer in each morphology type are depicted in Figure 5. The stick spectrum is converted into the continuous spectrum by the convolution with a Lorentzian function of 10 cm^{-1} full width at half-maximum. In the following, we summarize features of the hydrogen-bonded OH stretches in the calculated IR spectra.

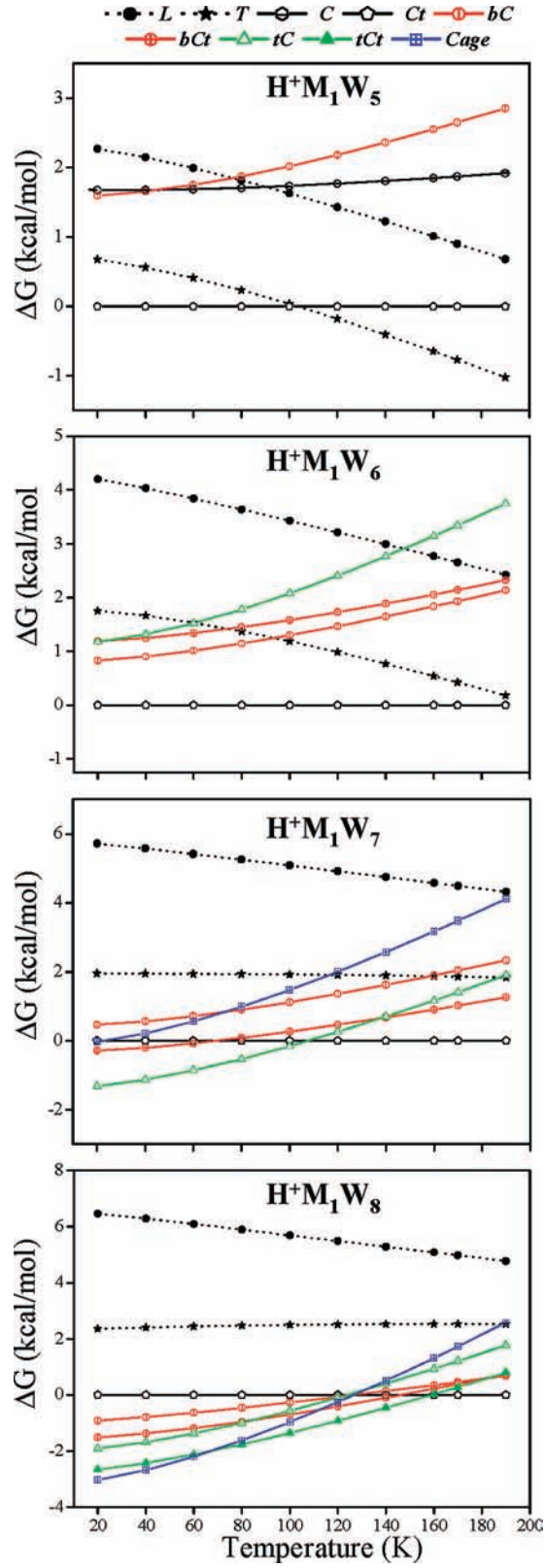

Figure 4. Temperature dependence of the relative Gibbs free energies of the different morphologies computed at B3LYP/6-31+G*. For simplicity, we only show the most stable isomer in each morphology as a representative. Note the preference of the "open" structures at elevated temperatures (see text).

A. L_n and T_n. The spectral features of L_n and T_n are similar to each other. The OH oscillators can be grouped accordingly to different solvation shells depending on their distance from the ion core (the vibration modes from OH oscillators at different

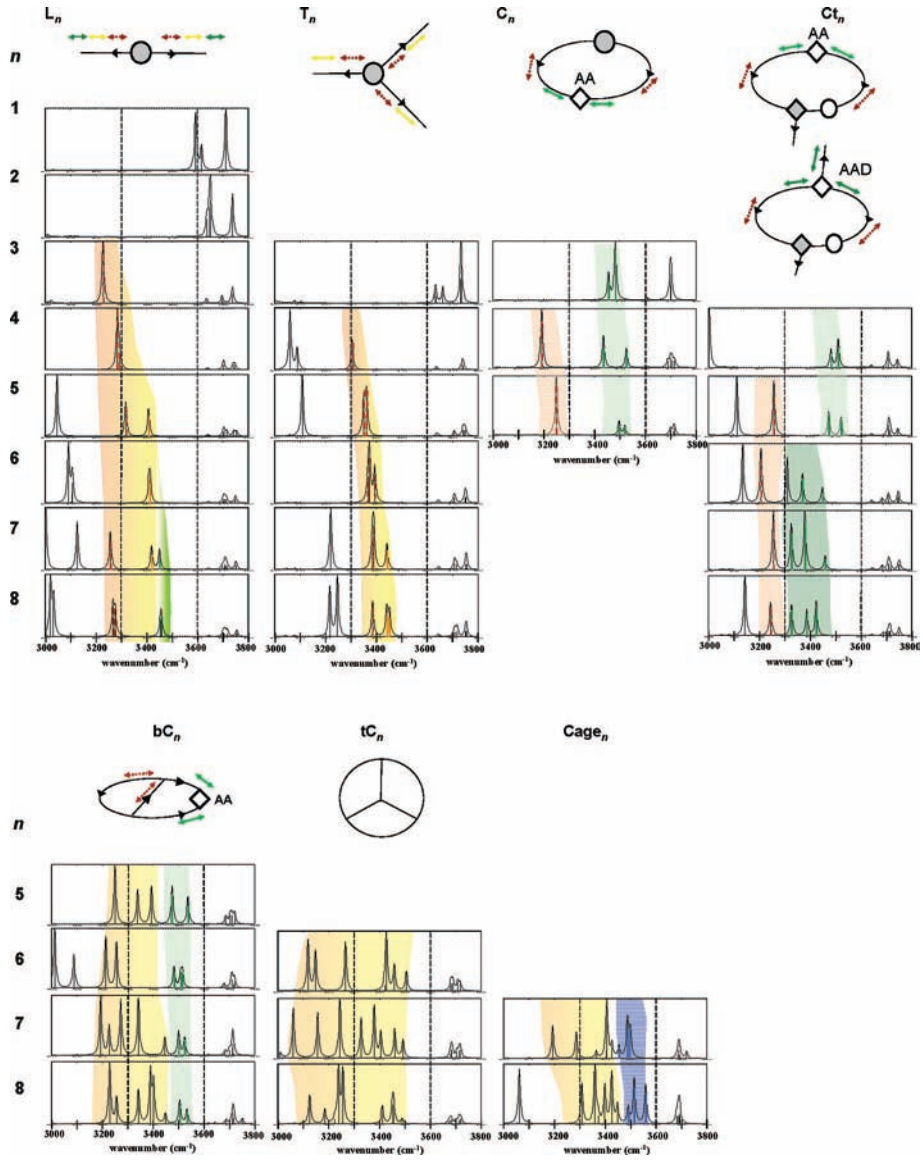

Figure 5. IR spectrum simulated by the most stable structure in each morphology shown in Figures 1 and 2. Calculations were carried out at the B3LYP/6-31+G* level with the scaling factor of 0.973. The vibrational bands are color-coded with the vibrational modes shown in the schematic representation of the morphologies, and the stripes are made for eye-guiding purposes. In the schematic representation of the morphologies, the oxygen atom in methanol/water is represented by an open circle/square, and the methyl groups and hydrogen atoms are omitted in the representation. An arrow indicates a hydrogen bond that binds two oxygen atoms. The direction of the arrow shows the donor−acceptor relation in the hydrogen bond. The gray circle/square represents the ion core. Detailed explanation can be found in ref 26.

solvation shells are color coded in Figure 5). For the linear isomers, the OH frequencies increase from ∼3220 cm^{-1} (first shell) to ∼3450 cm^{-1} (third shell). For the tree isomers, the OH frequencies increase from ∼3305 cm^{-1} (first shell) to ∼3450 cm^{-1} (second shell). This tendency is in line with the fact that the influence of the ion core on the solvent molecules decreases as the OH oscillators move away from the ion core.

Furthermore, among the OH oscillators on the same solvation shell, blue shifts are also evident as the cluster size grows. The origin of this blue-shifting trend can be understood by the charge transfer/delocalization from the ion core to the solvent molecules. We have analyzed the Mullikin charges on the solvent molecules and found out that the total amount of charge transferred to the solvent increases monotonically as the cluster size increases.

At $n = 7-8$, the shifts of the frequencies of these two distinct groups of the hydrogen-bonded OH bands are saturated at around 3250 and 3450 cm^{-1}. The similar trend in the linear and tree families has been reported for $H^+(MeOH)_m$.[26]

B. C_n and Ct_n. The IR spectra of C_n also show two blue-shifting groups in the hydrogen-bonded OH stretch region. In the isomers of these morphologies, the AA site tends to stay as far away from the ion core as possible. A pair of oscillators with of relatively higher frequency (marked in green in the figure) originates from the two water molecules next to the AA site. The low-frequency group (marked in orange) belongs to water molecules that are closer to the ion core. Both groups show slight blue-shifts with increase of the cluster size. The frequency shifts of these two groups are saturated at around 3500 and 3300 cm^{-1}, respectively. The spectra of Ct_n are more complicated. While the peaks from water near the AA site remain very similar to the cases in C_n, in larger clusters with two tails, OH stretching modes from water near the AAD site (marked in dark green) are red-shifted by about 100 cm^{-1} comparing to those modes in green.

C. Compact Structures. In the lower panels of Figure 5, we have shown the IR spectra of the more compact structures (bC_n, tC_n, and $cage_n$). Because of the strong coupling of the OH

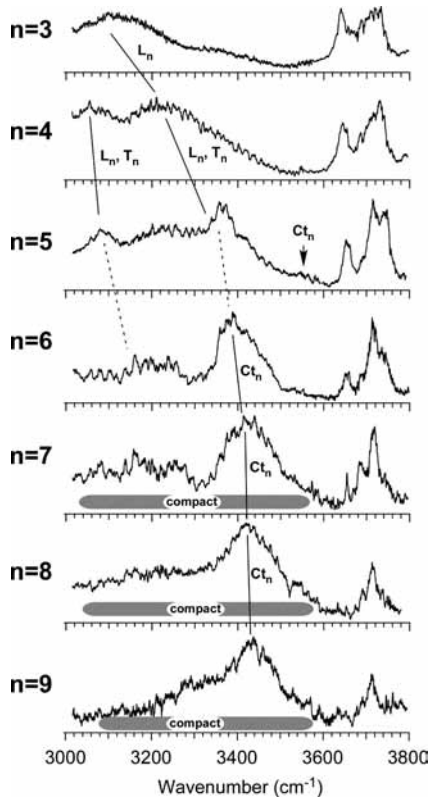

Figure 6. Observed IR spectra of $H^+M_1W_n$ ($n = 3-9$) in the 3-μm region. All the spectra were measured by monitoring the vibrational predissociation to the $H^+M_1W_{n-1}$ channel.

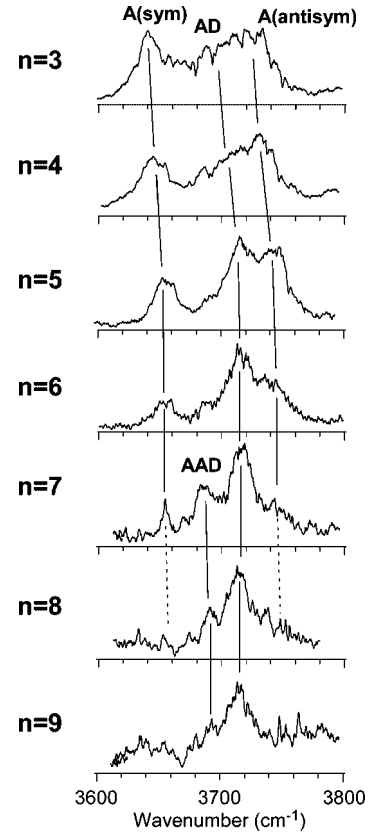

Figure 7. Observed IR spectra of $H^+M_1W_n$ ($n = 3-9$) in the free OH stretch region.

oscillators within the compact structures, their spectra between 3000 to 3600 cm^{-1} are less well resolved than the more open structures (L_n, T_n, and C_n). Nevertheless, there is a clear tendency that the further away a OH oscillator from the ion core, the higher the stretching frequencies. The high-frequency group of bC_n (in green) also originates from the two water molecules that are neighbors of the AA water. This group shows no change in the peak position with respect to those of open structures (C_n and Ct_n). The vibrational modes in tC_n are even more widely spread than those in bC_n. Since there is no AA water molecule in the tC_n structures, the notable difference from bC_n spectra is the missing of vibrational modes above 3500 cm^{-1}. In the cage structures, a new band (between 3500 and 3600 cm^{-1} - highlighted in green) emerges in the IR spectra of these structures and these are vibrational modes associated with the asymmetric stretching of the single acceptor−double donor (ADD) waters.

In summary, the vibration modes in open structures show a clear blue-shifting trend as the size of cluster increases. In the more compact forms, the OH oscillators tend to strongly coupled together leading to widely spread bands. Furthermore, we also notice that there are two sources of vibrational modes around and above 3500 cm^{-1}; one coming out from water next to AA sites and the other are associated with the asymmetric stretching of ADD water in the cage structures.

5. Comparison with the Observed IR Spectra with the Simulations. To compare with the IR simulations obtained in this study, we experimentally measured IR spectra of $H^+M_1W_n$ ($n = 3-9$) in the 3-μm region. The observed spectra are shown in Figure 6. All the spectra were obtained by monitoring the single water loss ($H^+M_1W_{n-1}$ fragment production), which follows to the vibrational excitation. The spectra of $n = 3-6$ are essentially the same as those reported by Chang and co-workers,[40] and they were remeasured for convenience of the comparison with the IR simulations. It is difficult to precisely estimate the temperature of the observed clusters. In comparison with the IR spectra of the temperature-controlled (or -determined) H^+W_n (77−180 K) reported by the Chang's group, the temperature of H^+W_n produced by our cluster ion source seems to be warmer. Then we roughly estimated the temperature of the clusters from our ion source to be ∼190 K.[7,9,48] Though this is not unequivocal evidence for the temperature determination, it would be reasonable to assume ∼190 K also for the temperature of the clusters in the present study.

In the observed spectra, relatively sharp bands due to the dangling OH stretches are seen above 3600 cm^{-1}, the region that is reproduced in the expanded scale in Figure 7, and much broader bands of the hydrogen-bonded OH stretches appear in the 3000−3600-cm^{-1} region.

In $n = 3-5$, two broadened band series, which show blue-shifts with increase of the cluster size, characterize the spectra. One series begins to appear at ∼3100 cm^{-1} in $n = 3$. This series gradually shifts to the blue side up to $n = 5$, and the band shift is saturated at ∼3400 cm^{-1}. The other series appears in $n = 4$ at ∼3050 cm^{-1} and shifts to ∼3080 cm^{-1} at $n = 5$. As seen in the previous subsection, the blue-shifting bands are characteristic to the L_n and T_n morphologies, and the appearance of these series is an indication of the dominant contributions of these two morphologies in the small-sized clusters. This is consistent with the spectral features in the dangling OH stretch region. The main features in the dangling OH stretch spectra of $n = 3-5$ are attributed to the symmetric and antisymmetric OH stretch bands of single acceptor (A) waters. The A waters locate at terminals of one-dimensional H-bond chains, and they are characteristic to L_n and T_n. In $n = 5$, the enhancement of the dangling OH stretch band of the AD water, which appears in

between the two dangling OH stretches of the A water, is clearly seen. This is attributed to the beginning of the contribution the Ct_n morphology, where the AD waters are dominant over the terminal A water. The contribution of the Ct_n morphology at $n = 5$ is also supported by the Gibbs energy evaluation at ~190 K, as shown in Figure 4. By consideration of the coexistence of the Ct_n morphology at $n = 5$, the extension of the H-bonded OH stretch absorption up to ~3600 cm^{-1} is attributed to the H-bonded OH stretches neighboring to the AA site, which is characteristic to Ct_n in $n \leq 5$. The dominance of L_n and T_n morphologies in $n < 5$ and coexistence of the Ct_n morphology at $n = 5$ have also been concluded in the previous study by Chang and co-workers,[40] though the cluster temperature in their study (170 K) would be colder than that in the present study (~190 K).

In $n = 6-7$, the dangling OH stretch bands of the A water remarkably diminish while those of the AD water become dominant. These spectral changes indicate that the L_n and T_n are no longer major isomers, but the Ct_n morphology becomes dominant in this size region, as suggested by the Gibbs energy evaluations in Figure 4. The Ct_n morphology in $n \geq 6$ is characterized by the strong bands at ~3400 cm^{-1}, which are due to the H-bonded OH stretch neighboring to the AAD water. The most prominent feature at 3400 cm^{-1} in the observed spectra of $n \geq 6$ is then mainly attributed to the Ct_n morphology with the possible minor contribution of the L_n and T_n morphologies, which also have the strong bands in the same region. All of the H-bonded OH bands of the L_n, T_n, and Ct_n morphologies of $n \geq 6$ are expected to appear below 3500 cm^{-1}. Then, a clear gap appears in between the H-bonded OH and dangling OH stretches in the spectrum of $n = 6$, while the H-bonded OH bands extend to the lower frequency region. In $n \geq 7$, on the other hand, the H-bonded OH stretch absorption extends up to the ~3600 cm^{-1} again, and a new feature simultaneously begins to appear in the dangling OH stretch region. The latter is assigned to the AAD water, which is characteristic to the more "compact" morphologies (bC_n, tC_n, and $Cage_n$). As was shown in the previous section, the compact morphologies have wide H-bonded OH absorption below 3600 cm^{-1}, and their contribution would be the origin of the extension of the H-bonded OH absorption to the higher frequency region in $n \geq 7$. The Gibbs energy evaluations also suggest that the compact morphologies become competitive in $n \geq 7$ at 190 K. Moreover, clear coexistence of the Ct_n and compact morphologies is expected in $n = 8$, while the L_n and T_n morphologies are less important. This is consistent with the observed features of the spectra of $n = 8$ and 9, the extremely broadened H-bonded absorption in the entire 3000−3600-cm^{-1} region with a clear peak at 3400 cm^{-1} and disappearance of the A water in the dangling OH stretch region.

V. Conclusion

Extensive DFT calculations of the protonated methanol−water mixed clusters were carried out to probe the morphological development of the hydrogen bond network in the mixed cluster system. It was shown that numerous structural isomers of different morphological motifs compete at the finite temperature. The hydrogen-bonded OH stretch bands in the observed IR spectra of the size-selected clusters were assigned by the spectral simulations on the basis of the energy-optimized structures. The excess proton location in the mixed clusters was examined. The preferentially protonated site changes from the methanol site in the simple linear chain structures to the water site in the 3-dimensionla cage structures. These results clearly demonstrated the correlation between the protonated site and the cluster morphology, which reflects the difference between the maximum coordination numbers of the methanol and water protonated ion cores.

Acknowledgment. This work was supported in part by Nanyang Technological University and Ministry of Education of Singapore under URC Grants (RG34/05 and RG57/05) and by the Grant-in-Aid for Scientific Research (KAKENHI) on Priority Areas "Molecular Science for Supra Functional Systems" [477] from MEXT, Japan, and Project Nos. 19205001 and 20550005 from JSPS, Japan.

Supporting Information Available: The complete list of the isomers of $H^+(MeOH)_1(H_2O)_n$ ($n = 1-8$) along with their relative energies. This material is available free of charge via the Internet at http://pubs.acs.org.

References and Notes

(1) Buck, U.; Huisken, F. *Chem. Rev.* **2000**, *100*, 3863.
(2) Meot-Ner (Mautner) , M. *Chem. Rev.* **2005**, *105*, 213.
(3) Lisy, J. M. *J. Chem. Phys.* **2006**, *125*, 132302.
(4) Yeh, L. I.; Okumura, M.; Myers, J. D.; Price, J. M.; Lee, Y. T. *J. Chem. Phys.* **1989**, *91*, 7319.
(5) Jiang, J. C.; Wang, Y. S.; Chang, H. C.; Lin, S. H.; Lee, Y. T.; Niedner-Schatteburg, G.; Chang, H.-C. *J. Am. Chem. Soc.* **2000**, *122*, 1398.
(6) Fridgen, T. D.; McMahon, T. B.; MacAleese, L.; Lemaire, J.; Maitre, P. *J. Phys. Chem. A* **2004**, *108*, 9008.
(7) Miyazaki, M.; Fujii, A.; Ebata, T.; Mikami, N. *Science* **2004**, *304*, 1134.
(8) Shin, J. -W.; Hammer, N. I.; Diken, E. G.; Johnson, M. A.; Walters, R. S.; Jaeger, T. D.; Duncan, M. A.; Christie, R. A.; Jordan, K. D. *Science* **2004**, *304*, 1137.
(9) Wu, C. C.; Lin, C. K.; Chang, H.-C.; Jiang, J. C.; Kuo, J. L.; Klein, M. L. *J. Chem. Phys.* **2005**, *122*, 074315.
(10) Lin, C.-K.; Wu, C.-C.; Wang, Y.-S.; Lee, Y. T.; Chang, H.-C.; Kuo, J.-L.; Klein, M. L. *Phys. Chem. Chem. Phys.* **2005**, *7*, 938.
(11) Chang, H.-C.; Wu, C.-C.; Kuo, J.-L. *Int. Rev. Phys. Chem.* **2005**, *24*, 553.
(12) Headrick, J. M.; Diken, E. G.; Walters, R. S.; Hammer, N. I.; Christie, R. A.; Cui, J.; Myshakin, E. M.; Duncan, M. A.; Johnson, M. A.; Jordan, K. D. *Science* **2005**, *303*, 1765.
(13) Mizuse, K.; Fujii, A.; Mikami, N. *J. Chem. Phys.* **2007**, *126*, 231101.
(14) Wales, D. J.; Hodges, M. P. *Chem. Phys. Lett.* **1998**, *286*, 65.
(15) Svanberg, M.; Pettersson, J. B. C. *J. Phys. Chem. A* **1998**, *102*, 1865.
(16) Kuo, J. L.; Klein, M. L. *J. Chem. Phys.* **2005**, *122*, 024516.
(17) Mella, M.; Kuo, J. L.; Clary, D. C.; Klein, M. L. *Phys. Chem. Chem. Phys.* **2005**, *7*, 2324.
(18) James, T.; Wales, D. J. *J. Chem. Phys.* **2005**, *122*, 134306.
(19) Iyengar, S. S.; Petersen, M. K.; Day, T. J. F.; Burnham, C. J.; Teige, V. E.; Voth, G. A. *J. Chem. Phys.* **2005**, *123*, 084309.
(20) Singh, N. J.; Park, M.; Min, S. K.; Suh, S. B.; Kim, K. S. *Angew. Chem., Int. Ed.* **2006**, *45*, 3795.
(21) Iyengar, S. S. *J. Chem. Phys.* **2007**, *126*, 216101.
(22) Luo, Y.; Maeda, S.; Ohno, K. *J. Phys. Chem. A* **2007**, *111*, 10732.
(23) Chang, H.-C.; Jiang, J.-C.; Lin, S. H.; Lee, Y. T.; Chang, H.-C. *J. Phys. Chem. A* **1999**, *103*, 2941.
(24) Chang, H.-C.; Jiang, J.-C.; Chang, H.-C.; Wang, L. R.; Lee, Y. T. *Isr. J. Chem.* **1999**, *39*, 231.
(25) Fujii, A.; Enomoto, S.; Miyazaki, M.; Mikami, N. *J. Phys. Chem. A* **2005**, *109*, 138.
(26) Kuo, J. L.; Fujii, A.; Mikami, N. *J. Phys. Chem. A* **2007**, *111*, 9438.
(27) Wakisaka, A.; Abdoul-Carime, H.; Yamamoto, Y.; Kiyozumi, Y. *J. Chem. Soc., Faraday Trans.* **1998**, *94*, 369.
(28) Dixit, S.; Crain, J.; Poon, W. C. K.; Finney, J. L.; Soper, A. K. *Nature* **2002**, *416*, 829.
(29) Guo, J. H.; Luo, Y.; Augustsson, A.; Kashtanov, S.; Rubensson, J. E.; Shuh, D. K.; Åren, H.; Nordgren, J. *Phys. Rev. Lett.* **2003**, *91*, 157401.
(30) Kebarle, P.; Haynes, R. M.; Collins, J. G. *J. Am. Chem. Soc.* **1967**, *89*, 5753.
(31) Stace, A. J.; Shukla, A. K. *J. Am. Chem. Soc.* **1982**, *104*, 5314.
(32) Stace, A. J.; Moore, C. *J. Am. Chem. Soc.* **1983**, *105*, 1814.
(33) Meot-Ner (Mautner) , M *J. Am. Chem. Soc.* **1986**, *108*, 6189.
(34) Shi, Z.; Wei, S.; Ford, J. V.; Castleman, A. W., Jr *Chem. Phys. Lett.* **1992**, *200*, 142.

(35) Zhang, X.; Castleman, A. W, Jr *J. Chem. Phys.* **1994**, *101*, 1157.
(36) Herron, W. J.; Coolbaugh, M. T.; Vaidyanathan, G.; Peifer, W. R.; Garvey, J. F. *J. Am. Chem. Soc.* **1992**, *114*, 3684.
(37) Lyktey, M. M. Y.; DeLeon, R. L.; Shores, K. S.; Furlani, T. R.; Garvey, J. F. *J. Phys. Chem. A* **2000**, *104*, 5197.
(38) Jackson, P. *Int. J. Mass Spectrom.* **2004**, *232*, 67.
(39) Chaudhuri, C.; Jiang, J. C.; Wang, X.; Lee, Y. T.; Chang, H.-C. *J. Chem. Phys.* **2000**, *112*, 7279.
(40) Wu, C. C.; Jiang, J. C.; Boo, D. W.; Lin, S. H.; Lee, Y. T.; Chang, H.-C. *J. Chem. Phys.* **2000**, *112*, 176.
(41) Jiang, J. C.; Chaudhuri, C.; Lee, Y. T.; Chang, H.-C. *J. Phys. Chem. A* **2002**, *106*, 10937.
(42) Wu, C.-C.; Chaudhuri, C.; Jiang, J. C.; Lee, Y. T.; Chang, H.-C. *J. Phys. Chem. A* **2004**, *108*, 2859.
(43) Suhara, K.; Fujii, A.; Mizuse, K.; Mikami, N.; Kuo, J. L. *J. Chem. Phys.* **2007**, *126*, 194306.
(44) Chang, H.-C.; Jiang, J.-C.; Hahndorf, I.; Lin, S. H.; Lee, Y. T.; Chang, H.-C. *J. Am. Chem. Soc.* **1999**, *121*, 4443.
(45) Diken, E. G.; Hammer, N. I.; Johnson, M. A.; Christie, R. A.; Jordan, K. D. *J. Chem. Phys.* **2005**, *123*, 164309.
(46) Hunter, E. P. L.; Lias, S. G. *J. Phys. Chem. Ref. Data* **1998**, *27*, 413.
(47) Frisch, M. J.; Trucks, G. W.; Schlegel, H. B.; Scuseria, G. E.; Robb, M. A.; Cheeseman, J. R.; Montgomery, Jr., J. A.; Vreven, T.; Kudin, K. N. ; Burant, J. C.; Millam, J. M.; Iyengar, S. S.; Tomasi, J.; Barone, V.; Mennucci, B.; Cossi, M.; Scalmani, G.; Rega, N.; Petersson, G. A.; Nakatsuji, H.; Hada, M.; Ehara, M.; Toyota, K.; Fukuda, R.; Hasegawa, J.; Ishida, M.; Nakajima, T.; Honda, Y.; Kitao, O.; Nakai, H.; Klene, M.; Li, X.; Knox, J. E.; Hratchian, H. P.; Cross, J. B.; Bakken, V.; Adamo, C.; Jaramillo, J.; Gomperts, R.; Stratmann, R. E.; Yazyev, O.; Austin, A. J.; Cammi, R.; Pomelli, C.; Ochterski, J. W.; Ayala, P. Y.; Morokuma, K.; Voth, G. A.; Salvador, P.; Dannenberg, J. J.; Zakrzewski, V. G.; Dapprich, S.; Daniels, A. D.; Strain, M. C.; Farkas, O.; Malick, D. K.; Rabuck, A. D.; Raghavachari, K.; Foresman, J. B.; Ortiz, J. V.; Cui, Q.; Baboul, A. G.; Clifford, S.; Cioslowski, J.; Stefanov, B. B.; Liu, G.; Liashenko, A.; Piskorz, P.; Komaromi, I.; Martin, R. L.; Fox, D. J.; Keith, T.; Al-Laham, M. A.; Peng, C. Y.; Nanayakkara, A.; Challacombe, M.; Gill, P. M. W.; Johnson, B.; Chen, W.; Wong, M. W.; Gonzalez, C.; Pople, J. A. ; *Gaussian 03*, revision D.01; Gaussian Inc.: Wallingford, CT, 2004.
(48) Wang, Y.-S.; Tsai, C.-H.; Lee, Y. T.; Chang, H.-C.; Jiang, J. C.; Asvany, O.; Schlemmer, S.; Gerlich, D. *J. Phys. Chem. A* **2003**, *107*, 4217.
(49) Singer, S. J.; McDonald, S.; Ojamäe, L. *J. Chem. Phys.* **2000**, *112*, 710.
(50) Ciobanu, C. V.; Ojamäe, L.; Shavitt, I.; Singer, S. J. *J. Chem. Phys.* **2000**, *113*, 5321.
(51) Christie, R. A.; Jordan, K. D. *J. Phys. Chem. B* **2002**, *106*, 8376.
(52) Wang, Y. S.; Jiang, J. C.; Cheng, C. -L.; Lin, S. H.; Lee, Y. T.; Chang, H.-C. *J. Chem. Phys.* **1997**, *107*, 9695.
(53) Wang, Y. S.; Chang, H. C.; Jiang, J. C.; Lin, S. H.; Lee, Y. T.; Chang, H. C. *J. Am. Chem. Soc.* **1998**, *120*, 8777.
(54) Jiang, J. C.; Chang, J.-C.; Wang, B.-C.; Lin, S. H.; Lee, Y. T.; Chang, H.-C. *Chem. Phys. Lett.* **1998**, *289*, 373.

JP8057299